Age-related changes in the plasticity and toughness of human cortical bone at multiple length scales

Elizabeth A. Zimmermann[a,b], Eric Schaible[b], Hrishikesh Bale[b], Holly D. Barth[a,b], Simon Y. Tang[c], Peter Reichert[b], Bjoern Busse[b], Tamara Alliston[c], Joel W. Ager III[b], and Robert O. Ritchie[a,b,1]

[a]Department of Materials Science and Engineering, University of California, Berkeley, CA 94720; [b]Materials Sciences Division, Lawrence Berkeley National Laboratory, Berkeley, CA 94720; and [c]Department of Orthopaedic Surgery, University of California, San Francisco, CA 94143

The structure of human cortical bone evolves over multiple length scales from its basic constituents of collagen and hydroxyapatite at the nanoscale to osteonal structures at near-millimeter dimensions, which all provide the basis for its mechanical properties. To resist fracture, bone's toughness is derived intrinsically through plasticity (e.g., fibrillar sliding) at structural scales typically below a micrometer and extrinsically (i.e., during crack growth) through mechanisms (e.g., crack deflection/bridging) generated at larger structural scales. Biological factors such as aging lead to a markedly increased fracture risk, which is often associated with an age-related loss in bone mass (*bone quantity*). However, we find that age-related structural changes can significantly degrade the fracture resistance (*bone quality*) over multiple length scales. Using in situ small-angle X-ray scattering and wide-angle X-ray diffraction to characterize submicrometer structural changes and synchrotron X-ray computed tomography and in situ fracture-toughness measurements in the scanning electron microscope to characterize effects at micrometer scales, we show how these age-related structural changes at differing size scales degrade both the intrinsic and extrinsic toughness of bone. Specifically, we attribute the loss in toughness to increased nonenzymatic collagen cross-linking, which suppresses plasticity at nanoscale dimensions, and to an increased osteonal density, which limits the potency of crack-bridging mechanisms at micrometer scales. The link between these processes is that the increased stiffness of the cross-linked collagen requires energy to be absorbed by "plastic" deformation at higher structural levels, which occurs by the process of microcracking.

Human cortical bone is a nanocomposite of collagen molecules and hydroxyapatite (HA) nanocrystals. However, its essential mechanical properties of stiffness (*ca.* 15–25 GPa), strength (*ca.* 100 MPa), and toughness ($\geq$5 MPa/m)[†] are not derived solely from the characteristic structure at the nanoscale, but rather at multiple length scales through bone's hierarchical architecture, which extends from molecular dimensions to the osteonal structures at near-millimeter levels. Indeed, salient mechanisms that strengthen and toughen bone can be identified at most of these length scales (Fig. 1) and can be usefully classified, as in many materials, in terms of intrinsic and extrinsic toughening mechanisms.

Intrinsic toughening mechanisms (1–6) enhance the inherent resistance of the material to fracture by inhibiting both the initiation and growth of cracks; in bone, they can be identified by plasticity (strictly inelasticity) mechanisms acting ahead of a crack and derived primarily at submicrometer length scales (Fig. 1). Extrinsic toughening mechanisms (7, 8), conversely, act primarily in the crack wake to inhibit crack growth by "shielding" it from the applied stresses. In bone, they are created principally by the interaction of growing cracks with the osteonal structures; as such, they are derived at much larger length scales in the range of tens to hundreds of micrometers.

Aging markedly increases the risk of fracture in bone. Although a major reason is the age-related loss in bone-mineral density (*bone quantity*) (9, 10), recent studies show that the structure and properties of bone specifically degrade with age, independent of the bone-mineral density (11), an issue of *bone quality*. Indeed, a deterioration in the bone toughness has been corre-

lated with aging (12, 13), as a result of a variety of nano- and/or microstructural changes including progressively larger osteonal dimensions and densities (14), increased nonenzymatic cross-link densities (15), and increased microcracking. In human cortical bone, cross-links occur in two forms: (*i*) enzymatic cross-links—as immature intrafibrillar (dehydrodihydroxynorleucine and dehydrohydroxylysinonorleucine) and mature interfibrillar (pyridinoline and pyrrole), and (*ii*) nonenzymatic advanced glycation end products (AGEs), such as pentosidine, that form both intra- and interfibrillar links along the collagen backbone (16). Although the level of enzymatic cross-links stabilizes around 10–15 y of age (17, 18), AGEs can increase up to fivefold with age (15, 18, 19), which has been correlated to reduced bone toughness and fracture resistance (20–23). Similarly, excessive remodeling with age increases the osteonal density in human cortical bone; this governs the degree of microcracking and in turn affects the development of crack bridges, which provide a major source of toughening at micrometer-scale levels and above (12).

In this work, we examine the role of aging on the mechanical properties of human cortical bone at multiple structural hierarchies using a set of samples from the same donors, by relating significant age-related structural changes to a degradation in specific toughening mechanisms detrimental to fracture resistance that arise at length scales from approximately tens of nanometers to hundreds of micrometers.

Results

Mechanical Properties. We examined the in vitro strength and toughness properties of hydrated human cortical bone samples from diaphyses of fresh-frozen humeri from young and old groups (young, 34–41 y old, $N = 7$; aged, 85–99 y old, $N = 6$). Middle-aged bone (61–69 y old, $N = 5$) was additionally evaluated for toughness measurements. Strength properties, determined from the three-point bending of unnotched beams, showed a 5% loss in yield strength and a 10% loss in peak strength with age (Fig. 2*A*). Corresponding fracture-toughness properties, presented in the form of stress-intensity K-based crack-resistance curves (R curves)[‡]
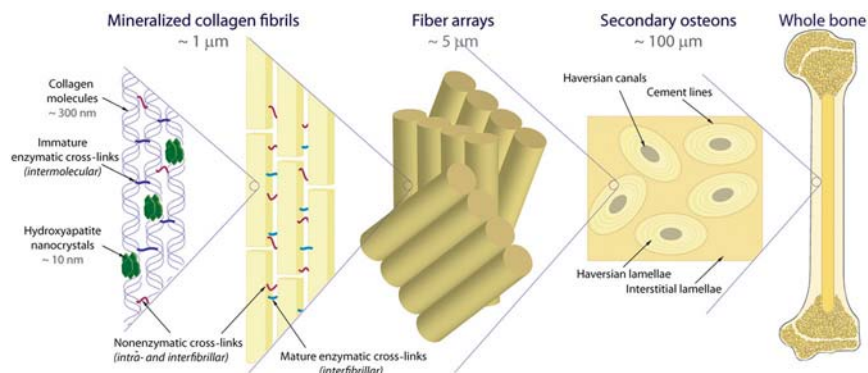
Fig. 1. Each level of the hierarchical structure influences the deformation and fracture of human cortical bone; the smaller levels affect the intrinsic toughness, whereas the higher length scales impact the extrinsic toughness. At the nanoscale, the polymeric nature of the collagen molecules allows them to uncoil and slide with respect to one another by breaking sacrificial bonds that absorb energy (2, 6). Sacrificial bonding also exists within higher levels of the hierarchy through shearing/stretching of the interfibrillar matrix and between fibrils (fibrillar sliding) (1, 3, 4). The process of microcracking can act as a plasticity mechanism by dissipating energy at coarser length scales typically exceeding several micrometers (5). Extrinsic mechanisms primarily act at the microstructural level by the interaction of growing cracks with the osteons; the weak boundaries in the secondary osteons absorb energy by microcracking during crack growth to toughen the structure mainly via crack bridging and crack deflection/twist (7, 8, 12).

in Fig. 2*B*, reveal a progressive loss in both the crack initiation and growth toughnesses in the longitudinal orientation with age. These latter data represent the current measurements on small cracks sized below approximately 500 µm, performed in situ in the environmental scanning electron microscope (ESEM), together with our previous ex situ measurements (12) on the same bone, where crack sizes were an order of magnitude larger. Because the combined R curves plotted in Fig. 2*B* indicate that the crack-growth toughness (i.e., slope of the R curve) is dependent upon the extent of crack extension, we measured this toughness from the slope of regression lines through each entire dataset but at larger crack extensions along the steady-state region of the curves. Based on these measurements, it is apparent that the toughness of the aged bone is over four times smaller than that of the young bone.

Structural Characterization at Micrometer Scales and Above. From in situ ESEM and ex situ 3D synchrotron X-ray computed tomography, the fracture surfaces were seen to be relatively smooth in the longitudinal orientation with crack paths showing extensive evidence of microcrack formation nominally parallel to, and ahead of, the growing crack (Fig. 3). The intact regions between the microcracks and the main growing crack result in the formation of "uncracked-ligament bridges" to provide a source of extrinsic toughening by carrying load that would otherwise be used to further crack growth. As reported previously, we found smaller and fewer crack bridges in the aged bone (Fig. 3) (12), resulting in a reduced contribution to the crack-growth toughness with age.

Three-dimensional X-ray computed tomography was also used to characterize the number and size of osteons in young and aged bone. Fig. 4 demonstrates the dramatically higher number of osteons in aged bone; in fact, the aged sample has nearly three times the osteonal density, defined as the number of osteons per unit bone area, consistent with reports elsewhere (24). The higher osteon density in aged bone supports the notion that a growing crack will have more cement lines at which microcracks can form, resulting in both smaller crack bridges and a lower crack-growth toughness.

Structural Characterization at Submicrometer Scales. To examine the corresponding intrinsic behavior at smaller (submicrometer) dimensions, we performed in situ high-flux synchrotron X-ray scattering experiments on uniaxial tensile specimens to study the mechanical behavior of the individual constituents of bone (Fig. 5).

Results from the small-angle X-ray scattering (SAXS) and wide-angle X-ray diffraction (WAXD) experiments are shown

as strains in the mineralized collagen fibrils (Fig. 5*A*) and mineral[§] (Fig. 5*B*) as a function of the macroscopic strain applied to the sample (i.e., tissue strain). For a given tissue strain, the strain in the mineralized collagen fibrils is more than 25% lower in aged bone (Fig. 5*D*) than in young bone, implying that the fibrils have become stiffer with age. (The SAXS/WAXD results reveal that the aged fibrils are stiffer because, for a given tissue strain, the collagen fibrils in young bone have a higher strain and thus absorb more energy through deformation at this structural level.)

For the stiffness of the fibrils to change with age, structural changes must be occurring at this level. To examine changes to the collagen environment with age, we quantified the collagen cross-linking due to nonenzymatic glycation—i.e., AGEs (Fig. 6). Consistent with the literature (15, 18), our results show a higher level of AGEs in aged bone than in young bone (Fig. 6). The SAXS/WAXD observations clearly indicate that these increased levels of nonenzymatic cross-links with age stiffen the collagen fibrils, thereby affecting the plasticity of the bone.

Discussion
The mechanisms of fracture resistance in human cortical bone derived over a range of length scales from molecular levels to near-millimeter dimensions are individually related to nano/microstructural features in the bone-matrix structure. These features degrade with biological aging and lead to a deterioration in the bone strength and toughness. Our macroscopic mechanical property measurements demonstrate that over the age range of about 34–99 y, there is a definite loss in bone quality affecting the fracture risk; specifically, there is a reduction in bone strength, initially as a loss in plasticity and subsequently in peak strength, and a corresponding significant decrease in fracture toughness, respectively, for crack initiation and crack growth (Fig. 2). However, the origin of these properties and their biological degradation reside at very different length scales.

Phenomena at Submicrometer Length Scales. Mineralized collagen fibrils, the basic building blocks of the bone matrix, consist of a self-assembly of collagen molecules and HA platelets. At this length scale, bone deforms by stretching/unwinding of individual collagen molecules (25, 26) and deformation of the mineral's crystalline lattice, which is primarily deposited in the gaps between the collagen molecules' 67-nm stagger.
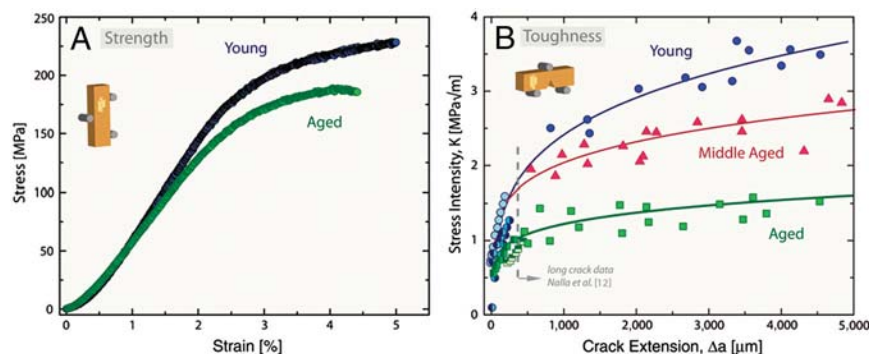
ENGINEERING

APPLIED BIOLOGICAL
SCIENCES

Fig. 2. In vitro mechanical properties of human cortical bone in 25 °C HBSS as a function of age showing (*A*) strength and (*B*) fracture-toughness R-curve properties for the young, middle-aged, and aged groups. The R-curve results encompass (long-crack growth) previous data, measured using crack sizes from approximately 500 μm to several millimeters (12), in addition to the current results on realistically short-crack extensions (<500 μm) performed in situ in the ESEM. The inset schematics describe the orientation of the osteons with respect to the sample geometry.

At the next length scale, the mechanical properties of the mineralized collagen fibril reflect the composite deformation of the collagen and HA. Within the fibrils, sliding at the HA/collagen interface (27), intermolecular cross-linking (16, 28, 29), and sacrificial bonding (3) constrain molecular stretching and provide the basis for the increased apparent strength of the collagen molecules without catastrophic failure of either component. The molecular behavior of the protein and mineral phases (fibrillar sliding) within a fibril enables a large regime of dissipative deformation once plastic yielding begins in mineralized tissues (4, 30, 31) and other biological materials (32). This model of load transfer represents the principal plasticity mechanism at this length scale. As in most materials, plasticity provides a major contribution to the intrinsic toughness by dissipating energy and forming "plastic zones" surrounding incipient cracks that further serve to blunt crack tips, thereby reducing the driving force (i.e., stress intensity) for crack propagation.

We find here that the strength and plasticity of bone are clearly degraded with age. The current in situ SAXS/WAXD studies provide experimental evidence of intrinsic mechanical degradation at the collagen fibril length scale; the results indicate that, for a given strain applied to the bone tissue, the strain carried by the collagen fibrils is significantly less, by some 25%, in aged bone compared to young (Fig. 5*A*). The origin of this stiffening of the collagen with age, though, can be associated with an even lower level of the hierarchy.

These conclusions are completely consistent with cross-linking measurements in this study (Fig. 6), and elsewhere (15, 18), that demonstrate that aging results in increased AGEs cross-links. These act to degrade the structural integrity of the fibrils by stiffening them to restrict fibrillar sliding[¶] (plasticity) and consequently degrade the ductility, strength, and intrinsic toughness of the bone. Further, our results are consistent with computational models of fibril deformation (28, 29, 33), which predict an inhibition of fibrillar sliding with cross-linking, and with experiments (22) showing a reduced toughness in bone glycated in vitro.

Taken as a whole, the evidence at submicrometer length scales strongly suggests that aging results in changes to the collagen environment, which specifically act to constrain the fibril's capacity to deform. The loss in plasticity at these nanometer length scales directly degrades the intrinsic toughness, thereby contributing to the increased fracture risk.

Phenomena at Micro to Near-Millimeter Length Scales. Another contribution to the fracture resistance of bone, however, is at much coarser length scales in the range of tens to hundreds of micrometers and involves mechanisms of extrinsic toughening that inhibit the growth of cracks. The primary driver for these mechanisms is the nature of the crack path and how it interacts with the bone-matrix structure. Two salient toughening mechanisms can be identified (7, 8): crack bridging and crack defection/twist. Several structural features (such as osteocyte lacunae, porosity, etc.; ref. 34) can deflect the crack path, but it is the largest features, specifically the secondary osteons, that are the most effective[‖] (7, 35, 36). The key feature is the hyper-mineralized osteonal boundaries (i.e., cement lines) that act as primary locations for microcracking. In the longitudinal orientation under study here, microcracks largely form parallel to or ahead of the main growing crack and result in the formation of uncracked-ligament bridges (Fig. 3). (These are simply uncracked regions in the wake of the main crack tip. They are not ligaments in the anatomical sense.) Detailed 2D ESEM and 3D computed X-ray tomography studies show that, in general, the size and frequency of these crack bridges are much lower in older bone (Fig. 3). We believe that the diminished crack bridging is the result of increased osteonal density and decreased size (Fig. 4), which is characteristic of older bone due to a higher rate of turnover. As the nominal size of the uncracked ligaments scales with the 3D osteonal spacing, the increased osteonal density leads to smaller and less frequent crack bridges. The marked reduction in the slope of the fracture-toughness R curves with age (Fig. 2*B*) is completely consistent with this diminished contribution from extrinsic toughening by crack bridging.

Coupling of Phenomena Across Length Scales. We observe intrinsic toughening in cortical bone by fibrillar sliding plasticity mechanisms at nanoscale levels and extrinsic toughening principally by crack deflection and bridging at length scales three orders of magnitude or so larger. We have direct evidence that aging leads to a suppression of fibrillar sliding associated with increased collagen cross-linking at molecular levels. It is intriguing to contemplate whether these multiscale mechanisms are coupled. We believe one route is through the mechanism of microcracking, which serves as a plasticity mechanism, a source of toughening as it induces both crack deflection and bridging, and may well initiate the signaling processes that promote bone remodeling (37). In this regard, it is pertinent to note that the SAXS/WAXD data in Fig. 5*A* show that the strain in the mineralized collagen fibrils

---

[¶]In Fig. 5*A*, the fibril strain vs. tissue strain curve is linear until the yield point. Once the samples begin to yield (at *ca.* 1% strain), the young and aged bones begin to deviate from linearity, which is much more apparent in the young bone. The nonlinearity may represent decoupling of the fibrils (4, 31). The fact that aged bone has a smaller degree of nonlinearity demonstrates the ability of nonenzymatic cross-links to inhibit fibrillar sliding past the yield point.

[‖]Larger-scale structural features, such as the interfaces (cement lines) of the osteonal structures, invariably result in far more substantial deflections of the crack path as compared to smaller structural features such as osteocyte lacunae and porosity; they accordingly have a more significant effect in enhancing the crack-growth toughness (35).
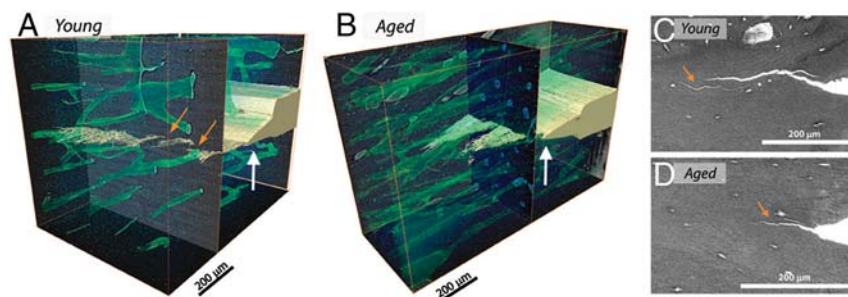
Fig. 3. (*A* and *B*) X-ray computed microtomography of young and aged bone samples show 3D images of the crack profile after roughly 500 μm of crack growth from a razor-sharpened notch (white arrows). (*C* and *D*) SEM images during small-crack R-curve experiments confirm the presence of large-crack bridges (other arrows) in young bone and smaller bridges in aged bone. The increased osteonal density in older bone leads to smaller and less frequent crack bridges and correlates with the marked reduction in the slope of the R curves with age.

in young bone is not that much less than the applied tissue strain (dotted line); this implies that the applied loads are being transferred far more effectively to the nanostructural length scales in young bone than aged bone, consistent with plasticity occurring by fibrillar sliding. In aged bone, conversely, this mechanism is clearly less effective because the fibrillar strains are significantly lower than the tissue strain. Consequently, the tissue deformation in aged bone must be accommodated by mechanisms occurring at higher structural levels to compensate for the lack of plasticity in the mineralized collagen fibrils. Indeed, our observations are consistent with models of deformation in hierarchical structures (28, 38) and by ribosylating bone samples to induce nonenzymatic glycation in vitro, which was found to decrease the bone's ability to dissipate energy postyield (22, 39, 40).

A higher incidence of microcracking in aged bone (41, 42), arising from nonenzymatic cross-links at the molecular and fibrillar level (40), is known to result in the formation of smaller crack bridges and diminished extrinsic toughening in aged bone (12). Additionally, at submicrometer length scales, it is consistent with observations showing a higher incidence of pre- and postyield microcracks in bone samples with higher levels of ribosylation-induced AGEs (40).

Whereas we believe that increased nonenzymatic cross-linking plays a prime role in suppressing deformation at the fibrillar level (22, 33, 39, 40), at this size scale, additional age-related changes to the organic matrix (3, 43–46), the mineral size (47), and post-translational modifications to the collagen (23) may influence the material properties. Additionally, variability in both mineralization (48–50) and the local mineral content (51–53) due to disease or osteoporosis treatments are known to affect the mechanical properties and may play a role in aging. We believe that the age-related increase in microdamage originates at the fibrillar level; however, changes in the location (42) or nature (54, 55) of microcracking with age may further reveal how this role of microcracking contributes to the toughness. At higher structural levels, intracortical porosity (56–58) and an irregular collagen fibril orientation (59, 60) may additionally impact the mechanical properties.

Conclusion

Human cortical bone derives its strength and toughness from mechanisms that dissipate energy at many different structural length scales; by the same token, biological factors such as aging that impair bone quality also operate at these differing scales. In this study, we have partitioned these mechanisms into intrinsic toughening (plasticity) mechanisms such as fibrillar sliding that operate at dimensions typically below a micrometer, and extrinsic toughening (crack-tip shielding) mechanisms such as crack bridging that operate at dimensions often well above a micrometer. At the macroscopic level, aging compromises the strength, ductility (plasticity), and intrinsic toughness. Through a series of experimental multiscale structural and mechanical characterizations, we attribute this degradation to a series of coupled mechanisms starting at the lowest (molecular) hierarchical levels, by changing the deformation behavior of the mineralized collagen fibrils due to increased inter- and intrafibrillar cross-linking. The resulting elevated stiffness of the collagen negatively affects the bone's ability to plastically deform by fibrillar sliding, which then must be accommodated at higher structural levels, by increased microcracking. Coupled with an increased osteonal density in older bone, the higher density of microcracks in turn compromises the formation of crack bridges, which provide one of the main sources of extrinsic toughening in bone at length scales in the range of tens to hundreds of micrometers.

Materials and Methods

Sample Preparation. The cortical bone used in this study was from the diaphyses of fresh-frozen human humeri from several age groups, specifically young (34 y old, $N = 1$; 37 y old, $N = 4$; and 41 y old, $N = 2$) and aged (85 y old, $N = 3$; 91 y old, $N = 1$; and 99 y old, $N = 2$). Middle-aged bone (61 y old, $N = 1$; 69 y old, $N = 2$; and 69 y old, $N = 2$) was additionally evaluated for toughness measurements.

Strength and Toughness Testing. For strength and toughness testing, samples of bone with an approximately 2-mm width and 1.5-mm thickness were machined with a low-speed saw. The fracture-toughness samples contained a notch oriented with the nominal crack-growth direction parallel to the bone's long axis. Notches were cut with a low-speed diamond saw and then
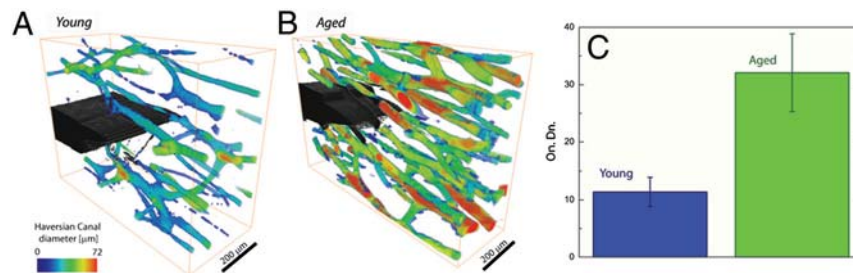

Fig. 4. X-ray computed tomography was also used to image the size and density of Haversian canals in (*A*) young and (*B*) aged human cortical bone (the color coding indicates the diameter of the Haversian canals). (*C*) Aged bone has nearly three times the osteonal density—i.e., number of osteons per unit bone area (On.Dn.)—as young bone, implying more cement lines for microcracks to initiate and smaller crack bridges during crack growth.
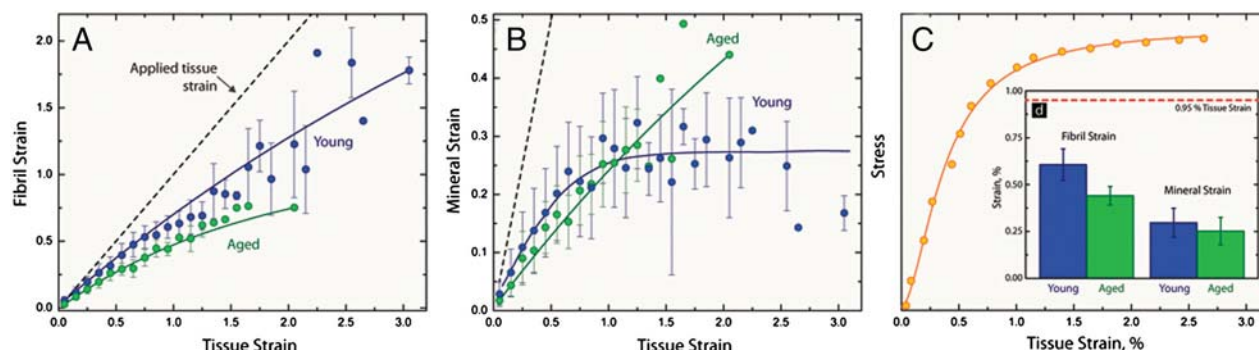
Fig. 5. The results of the (*A*) SAXS and (*B*) WAXD experiments for tensile testing of young and aged cortical bone samples in the longitudinal orientation. For each individual tensile test, the strain values were binned every 0.1% tissue strain; then, for each age group, the average and standard deviation of the binned values were calculated and are shown as the dots and error bars, respectively. *C* shows a representative stress–strain curve for the tensile tests. (*D*) At a fixed tissue strain, the individual strain in the fibrils is approximately 25% smaller in aged bone than young bone, although changes in the mineral strain are not significant.

sharpened with a razor blade that was continually irrigated with 1-μm diamond slurry producing micronotches with a root radius of approximately 3–5 μm and an initial crack length of $a \approx 1$ mm in accordance with American Society for Testing and Materials (ASTM) standards (61). The resulting toughness specimens were ground and polished to a 0.05-μm finish. All samples were stored in HBSS at 25 °C for at least 12 h prior to testing.

In accordance with ASTM standards (61, 62), a three-point bending configuration was used for the strength and toughness** (i.e., R curve) tests with a displacement rate of 0.55 μm/s in 25 °C HBSS. To make such measurements while simultaneously imaging the initiation and growth of cracks in real time, in situ testing of HBSS-soaked samples was performed in a Hitachi S-4300SE/N ESEM (Hitachi America) at 25 °C using a Gatan Microtest 2-kN three-point bending stage (Gatan). Images of the crack path were obtained simultaneously in back-scattered electron mode at a voltage of 25 kV and a pressure of 35 Pa. These tests were used to define the early portion of the R curves. The total crack extensions were small (<500 μm) and as such physiologically relevant. R curve determination was limited to small-scale bridging conditions.

SAXS/WAXD Testing. Samples of human cortical bone were prepared with a low-speed saw and polished to a final dimension of roughly 15 mm × 1 mm × 200 μm, such that the long axes of the samples and bone were parallel. The samples were wrapped in HBSS-soaked gauze for at least 12 h prior to testing.

The samples were loaded in tension at a displacement rate of 1 μm/s in a custom-made rig with a 5-kg load cell (Omega, LC703-10). The rig was positioned in beamline 7.3.3 at the Advanced Light Source (ALS) synchrotron radiation facility (Lawrence Berkeley National Laboratory), such that SAXS/WAXD data were collected simultaneously with mechanical loading. (During mechanical testing, samples were exposed to X-rays for 0.5 s every 15 s, limiting the total X-ray exposure to 30 kGy to minimize its influence on the mechanical properties; ref. 35.) The testing was performed at 25 °C on continuously hydrated samples. A high-speed Pilatus detector and a Quantum CCD X-ray detector (Area Detector Systems Corporation) were positioned at approximately 4,100 and 250 mm from the sample, respectively, to collect SAXS and WAXD data.

The tissue strain was measured by imaging the change in spacing of horizontal lines marked on the sample's surface, which were later analyzed with image analysis software (National Instruments Vision Assistant 8.5); the lines' displacement was divided by the separation at zero load to determine the bulk tissue strain. The analysis software IGOR Pro (Wavemetrics) was used in conjunction with the custom macro NIKA (Jan Ilavsky, Argonne National Laboratory, Argonne, IL) to convert the 2D data to 1D. The sample-to-detector distance and beam center were calibrated with standards. The 2D SAXS and WAXD data were converted to 1D by radially integrating over a 10° sector and a 20-pixel-wide sector, respectively oriented parallel to the direction of loading. The first-order collagen peak and the (0002) HA peak were found by fitting the 1D datasets with a Gaussian function and a fourth-order poly-

nomial. The strain in the collagen fibrils and mineral were measured as the change in position of the corresponding peak's center divided by its location at zero load.

X-Ray Computed Microtomography. Synchrotron X-ray computed microtomography was performed at the ALS (beamline 8.3.2) to visualize the 3D distribution of secondary osteons and the crack path after R-curve testing. An incident X-ray energy of 18 keV was selected with an exposure time of 350 ms. The final spatial resolution was 1.8 μm per voxel. The datasets were reconstructed using the software Octopus (63) and 3D visualization was performed using Avizo™ software. Through a series of binary pixel open, close, and erode operations, the morphology of the bone volume was binarized. Calculations of the Haversian canal diameter were performed using a 3D ellipsoid fitting algorithm. The average osteonal density was derived from the ratio of the binary black pixels over the total image stack volume.

Accumulation of Advanced Glycation End Products. A fluorometric assay was performed to evaluate the extent of AGEs in the bone samples. A section of the humeral midshafts was demineralized using EDTA and then hydrolyzed using 6 N HCl (24 h, 110 °C). AGE content was determined using fluorescence readings taken using a microplate reader at the excitation wavelength of 370 nm and emission wavelength of 440 nm. These readings were standardized to a quinine-sulfate standard and then normalized to the amount of collagen present in each bone sample. The amount of collagen for each sample was determined based on the amount of hydroxyproline, the latter being determined using a chloramine-T colorimetric assay that recorded the absorbance of the hydrolysates against a commercially available hydroxyproline standard at the wavelength of 585 nm (64).
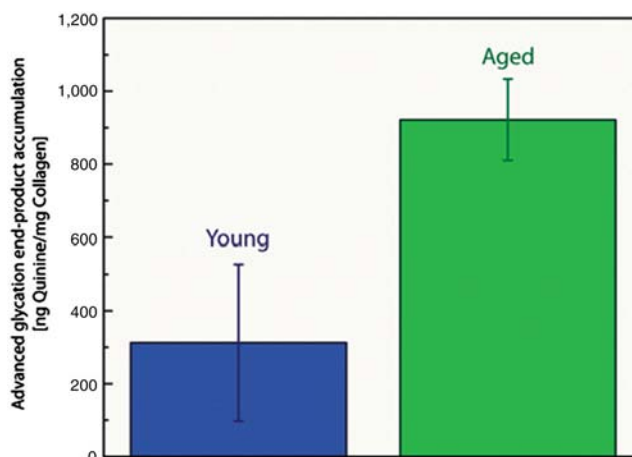

Fig. 6. The accumulation of AGEs was fluorimetrically quantified in the cortex of young and aged bone samples. These results indicate that the aged bone contained nearly three times as many fluorescent cross-links as the young bone.

**Although a nonlinear *J*-integral analysis is often recommended, a linear-elastic fracture mechanics (LEFM) analysis was used here (similar to the long-crack data of Nalla et al., ref. 12, presented in Fig. 2). The LEFM approach is justified by the fact that the plastic-zone size, calculated as $r_y \sim \frac{1}{2\pi}(K/\sigma_Y)^2$, where σ_Y is the yield stress (120 MPa), was small enough to achieve a state of small-scale yielding and plane strain in our samples.

Zimmermann et al.

1. Bailey AJ, Sims TJ, Avery NC, Miles CA (1993) Chemistry of collagen cross-links—glucose-mediated covalent cross-linking of type-IV collagen in lens capsules. *Biochem J* 296:489–496.
2. Buehler MJ (2007) Molecular nanomechanics of nascent bone: Fibrillar toughening by mineralization. *Nanotechnology* 18:295102.
3. Fantner GE, et al. (2005) Sacrificial bonds and hidden length dissipate energy as mineralized fibrils separate during bone fracture. *Nat Mater* 4:612–616.
4. Gupta HS, et al. (2006) Cooperative deformation of mineral and collagen in bone at the nanoscale. *Proc Natl Acad Sci USA* 103:17741–17746.
5. Nalla RK, Kruzic JJ, Ritchie RO (2004) On the origin of the toughness of mineralized tissue: Microcracking or crack bridging? *Bone* 34:790–798.
6. Thompson JB, et al. (2001) Bone indentation recovery time correlates with bond reforming time. *Nature* 414:773–776.
7. Koester KJ, Ager JW, Ritchie RO (2008) The true toughness of human cortical bone measured with realistically short cracks. *Nat Mater* 7:672–677.
8. Nalla RK, Kruzic JJ, Kinney JH, Ritchie RO (2005) Mechanistic aspects of fracture and R-curve behavior in human cortical bone. *Biomaterials* 26:217–231.
9. Marshall D, Johnell O, Wedel H (1996) Meta-analysis of how well measures of bone mineral density predict occurrence of osteoporotic fractures. *BMJ* 312:1254–1259.
10. Cummings SR, et al. (1993) Bone density at various sites for prediction of hip fractures. *Lancet* 341:72–75.
11. Hui SL, Slemenda CW, Johnston CC (1988) Age and bone mass as predictors of fracture in a prospective-study. *J Clin Invest* 81:1804–1809.
12. Nalla R, et al. (2006) Role of microstructure in the aging-related deterioration of the toughness of human cortical bone. *Mater Sci Eng C Mater Biol Appl* 26:1251–1260.
13. Zioupos P, Currey JD (1998) Changes in the stiffness, strength, and toughness of human cortical bone with age. *Bone* 22:57–66.
14. McCalden RW, McGeough JA, Barker MB, Courtbrown CM (1993) Age-related-changes in the tensile properties of cortical bone—the relative importance of changes in porosity, mineralization, and microstructure. *J Bone Joint Surg Am* 75A:1193–1205.
15. Sell DR, Monnier VM (1989) Structure elucidation of a senescence cross-link from human extracellular matrix. Implication of pentoses in the aging process. *J Biol Chem* 264:21597–21602.
16. Bailey AJ (2001) Molecular mechanisms of ageing in connective tissues. *Mech Ageing Dev* 122:735–755.
17. Eyre DR, Dickson IR, Vanness K (1988) Collagen cross-linking in human-bone and articular-cartilage—age-related-changes in the content of mature hydroxypyridinium residues. *Biochem J* 252:495–500.
18. Saito M, Marumo K, Fujii K, Ishioka N (1997) Single-column high-performance liquid chromatographic-fluorescence detection of immature, mature, and senescent cross-links of collagen. *Anal Biochem* 253:26–32.
19. Odetti P, et al. (2005) Advanced glycation end-products and bone loss during aging. *Ann N Y Acad Sci* 1043:710–717.
20. Wang X, Shen X, Li X, Agrawal CM (2002) Age-related changes in the collagen network and toughness of bone. *Bone* 31:1–7.
21. Ager JW, Balooch G, Ritchie RO (2006) Fracture, aging, and disease in bone. *J Mater Res* 21:1878–1892.
22. Vashishth D, et al. (2001) Influence of nonenzymatic glycation on biomechanical properties of cortical bone. *Bone* 28:195–201.
23. Garnero P, et al. (2006) Extracellular post-translational modifications of collagen are major determinants of biomechanical properties of fetal bovine cortical bone. *Bone* 38:300–309.
24. Busse B, et al. (2010) Reorganization of the femoral cortex due to age-, sex-, and endoprosthetic-related effects emphasized by osteonal dimensions and remodeling. *J Biomed Mater Res A* 92A:1440–1451.
25. Launey ME, Buehler MJ, Ritchie RO (2010) On the mechanistic origins of toughness in bone. *Annu Rev Mater Res* 40:25–53.
26. Ritchie RO, Buehler MJ, Hansma P (2009) Plasticity and toughness in bone. *Phys Today* 62:41–47.
27. Ji B, Gao H (2004) Mechanical properties of nanostructure of biological materials. *J Mech Phys Solids* 52:1963–1990.
28. Buehler MJ (2008) Nanomechanics of collagen fibrils under varying cross-link densities: Atomistic and continuum studies. *J Mech Behav Biomed Mater* 1:59–67.
29. Uzel SGM, Buehler MJ (2011) Molecular structure, mechanical behavior and failure mechanism of the C-terminal cross-link domain in type I collagen. *J Mech Behav Biomed Mater* 4:153–161.
30. Krauss S, et al. (2009) Inhomogeneous fibril stretching in antler starts after macroscopic yielding: Indication for a nanoscale toughening mechanism. *Bone* 44:1105–1110.
31. Gupta HS, et al. (2006) Fibrillar level fracture in bone beyond the yield point. *Int J Fract* 139:425–436.
32. Harrington MJ, Gupta HS, Fratzl P, Waite JH (2009) Collagen insulated from tensile damage by domains that unfold reversibly: In situ X-ray investigation of mechanical yield and damage repair in the mussel byssus. *J Struct Biol* 167:47–54.
33. Siegmund T, Allen MR, Burr DB (2008) Failure of mineralized collagen fibrils: Modeling the role of collagen cross-linking. *J Biomech* 41:1427–1435.
34. Currey JD (1962) Stress concentrations in bone. *Q J Microsc Sci* 103:111–133.
35. Barth HD, et al. (2010) On the effect of X-ray irradiation on the deformation and fracture behavior of human cortical bone. *Bone* 46:1475–1485.
36. Martin RB, Burr DB (1982) A hypothetical mechanism for the stimulationof osteonal remodeling by fatigue damage. *J Biomech* 15:137–139.
37. Hazenberg JG, et al. (2006) Microdamage: A cell transducing mechanism based on ruptured osteocyte processes. *J Biomech* 39:2096–2103.
38. Gao HJ (2006) Application of fracture mechanics concepts to hierarchical biomechanics of bone and bone-like materials. *Int J Fract* 138:101–137.
39. Tang SY, Zeenath U, Vashishth D (2007) Effects of non-enzymatic glycation on cancellous bone fragility. *Bone* 40:1144–1151.
40. Tang SY, Vashishth D (2010) Non-enzymatic glycation alters microdamage formation in human cancellous bone. *Bone* 46:148–154.
41. Mori S, Harruff R, Ambrosius W, Burr DB (1997) Trabecular bone volume and microdamage accumulation in the femoral heads of women with and without femoral neck fractures. *Bone* 21:521–526.
42. Schaffler MB, Choi K, Milgrom C (1995) Aging and matrix microdamage accumulation in human compact bone. *Bone* 17:521–525.
43. Burr DB (2002) The contribution of the organic matrix to bone's material properties. *Bone* 31:8–11.
44. Fratzl P, Gupta HS, Paschalis EP, Roschger P (2004) Structure and mechanical quality of the collagen-mineral nano-composite in bone. *J Mater Chem* 14:2115–2123.
45. Sroga GE, Karim L, Colón W, Vashishth D (2011) Biochemical characterization of major bone-matrix proteins using nanoscale-size bone samples and proteomics methodology. *Mol Cell Proteomics*, 10.1074/mcp.M110.006718.
46. Thurner PJ, et al. (2010) Osteopontin deficiency increases bone fragility but preserves bone mass. *Bone* 46:1564–1573.
47. Boskey AL, et al. (2005) Comparison of mineral quality and quantity in iliac crest biopsies from high- and low-turnover osteoporosis: An FT-IR microspectroscopic investigation. *Osteoporos Int* 16:2031–2038.
48. Currey JD, Brear K, Zioupos P (1996) The effects of ageing and changes in mineral content in degrading the toughness of human femora. *J Biomech* 29:257–260.
49. Landis WJ (1995) The strength of a calcified tissue depends in part on the molecular structure and organization of its constituent mineral crystals in their organic matrix. *Bone* 16:533–544.
50. Turner CH (2002) Biomechanics of bone: Determinants of skeletal fragility and bone quality. *Osteoporos Int* 13:97–104.
51. Boskey AL, Spevak L, Weinstein RS (2009) Spectroscopic markers of bone quality in alendronate-treated postmenopausal women. *Osteoporos Int* 20:793–800.
52. Kreider JM, Goldstein SA (2009) Trabecular bone mechanical properties in patients with fragility fractures. *Clin Orthop Relat Res* 467:1955–1963.
53. McCreadie BR, et al. (2006) Bone tissue compositional differences in women with and without osteoporotic fracture. *Bone* 39:1190–1195.
54. Diab T, Condon KW, Burr DB, Vashishth D (2006) Age-related change in the damage morphology of human cortical bone and its role in bone fragility. *Bone* 38:427–431.
55. Burr DB, et al. (1997) Bone microdamage and skeletal fragility in osteoporotic and stress fractures. *J Bone Miner Res* 12:6–15.
56. Kazakia GJ, Burghardt AJ, Link TM, Majumdar S (2011) Variations in morphological and biomechanical indices at the distal radius in subjects with identical BMD. *J Biomech* 44:257–266.
57. Nishiyama KK, et al. (2010) Postmenopausal women with osteopenia have higher cortical porosity and thinner cortices at the distal radius and tibia than women with normal aBMD: An in vivo HR-pQCT study. *J Bone Miner Res* 25:882–890.
58. Tang SY, Vashishth D (2011) The relative contributions of non-enzymatic glycation and cortical porosity on the fracture toughness of aging bone. *J Biomech* 44:330–336.
59. Ascenzi M-G, et al. (2003) Structural differences between "dark" and "bright" isolated human osteonic lamellae. *J Struct Biol* 141:22–33.
60. Portigliatti Barbos M, Bianco P, Ascenzi A, Boyde A (1984) Collagen orientation in compact bone: II. Distribution of lamellae in the whole of the human femoral shaft with reference to its mechanical properties. *Metab Bone Dis Relat Res* 5:309–315.
61. ASTM E1820-09. *Annual Book of ASTM Standards, Standard Test Method for Measurement of Fracture Toughness* (ASTM International, West Conshohocken, PA).
62. ASTM D790-10. *Annual Book of ASTM Standards, Standard Test Methods for Flexural Properties of Unreinforced and Reinforced Plastics and Electrical Insulating Materials* (ASTM International, West Conshohocken, PA).
63. Vlassenbroeck J, et al. (2007) Software tools for quantification of X-ray microtomography. *Nucl Instrum Methods Phys Res Sect A* 580:442–445.
64. Woessner JF (1961) The determination of hydroxyproline in tissue and protein samples containing small proportions of this imino acid. *Arch Biochem Biophys* 93:440–447.

ENGINEERING

APPLIED BIOLOGICAL SCIENCES